Optoelectronic and polaritonic devices using two dimensional van der Waals materials

By

Chung-Kuan (Andy) Lin

A dissertation submitted in partial satisfaction of the

requirements for the degree of

Master of Science

in

Engineering - Materials Science and Engineering

in the

Graduate Division

of the

University of California, Berkeley

Committee in charge:

Professor Feng Wang, Co-Chair
Professor Mark Asta, Co-Chair
Professor David Attwood
Professor Peidong Yang

Spring 2018

Abstract

Optoelectronic and polaritonic devices using two dimensional van der Waals materials

By

Chung-Kuan (Andy) Lin

Master of Science in Material Science and Engineering
University of California, Berkeley
Professor Feng Wang, Co-Chair
Professor Mark Asta, Co-Chair

Two dimensional van der Waals layered materials are semiconductors possessing intriguing properties, such as such strong absorption coefficients, large exciton binding energies, and high electron mobility. These properties enable us to engineer the materials to study new physics and advance device applications.

This thesis presents research in two main areas: (1) integrating 2D tungsten disulfide (WS_2) in a planar waveguide to study exciton-polaritons; and (2) utilizing black phosphorous as an ultrafast photodetector.

For part (1), we design a new platform to strongly couple two-dimensional materials with dielectric planar waveguides. The new method has several advantages: (1) all photonic elements are made of dielectric materials avoiding metal absorption in contrast to plasmonic designs, and (2) the light confinement is based on total internal reflection, leading to a small mode volume compared to distributed bragg reflecting mirrors. By transferring WS_2 monolayer onto designed planar waveguides, we demonstrate that the waveguide mode and the A-exciton mode of monolayer WS_2 can reach a strong coupling regime through analyzing the angle-resolved reflection spectra. A Rabi splitting of ~30meV is observed experimentally.

For part (2), we have achieved a high-speed photodetector made of black phosphorene with a bandwidth up to 10GHz. At the same time, the direct bandgap of black phosphorene gives large optical absorption and results in large photo-responsivity. The simplicity of the vertical structure also allows us to integrate it with an optical waveguide for telecommunication purposes.

Table of contents

Acknowledgements

Berkeley is a unique place to be and to enjoy doing research. Not only because every day we are surrounded by stimulating conversation and ideas, but people here care about what happens in the world and will fight for truth and ideals. I am grateful for all the teachers leading me to this path, bringing me to this day, and the Berkeley land that sustains us in every aspect.

I would like to thank Dr. Feng Wang for offering me the opportunity to join the lab and to pursue cutting-edge research. Feng teaches us by exampling himself; his boundless knowledge and rigor in pursuing science are inspiring. His deep understanding in physics pushes every intriguing scientific problem to its limits. It is a unique experience to work with him.

No scientist is an island. Over the years I have learned from and interacted with many bright and kind people. The scientist I am mostly indebted is probably Jason Horng. I work with Jason from the very first day. Jason has taught me many things—including how to construct physics pictures from mathematical basis, building optics, taking measurements and to read what data is trying to tell us. Jason is both a sharper thinker and a kind mentor.

After Jason left I came to work with Rai Takahashi and Patrick Gallagher. Rai's insistence and carefulness has been invaluable every step of the way, BP photodetector would not be successful without his knowledge on high-speed measurements and device fabrication. After Rai left, Patrick Gallagher guided me both on setting up optics and dealing with life.

The Birge B1 office would be very quiet if Iqbal Utama did not share his wisdom and tips in grad school, he's also good at giving useful advice when people are in dilemma; lunch time would be boring if Emma Regan did not share her insights and perspectives in life. Emma is also a good skier. I thank Chaw Keong Yong for sharing with me many useful optics techniques. Halleh Balch and Steve Drapcho are always cheerful and willing to share advices. My time in Birge would be much less colorful without many enthusiastic people, they are: Chan-Shan Yang, Sheng Wang, Sihan Zhao, Chenhao Jin and many other group members in ultrafast nano-optics lab.

Outside the lab there are many conspirators and the days in Berkeley and bay area would not be so much fun without conspiring those plans and get outdoors together. Cher-Chia (James) Yeh is the chief executive conspirator, he also made the best teammate when both of us exploring many unknowns and first-times. Fuyi Yang is another scientist I am indebted with. We have lots of conversation and debates in solid state physics, and she's very generous and charmingly quirky. Li-Wei Chen is always ready to recommend anyone a movie to dilute one's upset (or opposite). I would also like to thank Albert Lee, Fang-Chieh Chou, Nai-Wen Hu and many other people that I cannot possibly name here.

A few other teachers when I was in college also deserve a few words; Wen-Bin Jian (Professor in National Chiao Tung University) and Yen-Fu Lin (Now Professor at National Chung-Hsing Universty) graciously allowed me to touch their probe station and carried out some transport experiments when I was an undergrad kid (and luckily I did not destroy the equipment too much). Cheng Chin (Professor at UChicago) and Nai-Chang Yeh (Professor at Caltech) are generous and inspiring when I was working in their lab.

I would like to thank Professor Mark Asta, Professor David Attwood and Professor Peidong Yang for serving my thesis committee. Mark Asta is a wise scientific leader. He influenced me by exampling himself when dealing with problems in every aspect in an organized and logical way, he is also very generous in sharing advise. I am privileged to have the chance to take X-ray course with David Attwood, he is a respectful educator always looking after young people. He's also the founder and president of "Berkeley Medallion Association" while I am honored to be one of the member. Peidong is a sharper thinker that always ready to give critical opinion.

My first and most important teachers are my parents---Yu-Sheng Lin and Chih-Lan Ho. They've given me the chance and handed me the most important tools for the journey---Intelligence, diligence and compassion.

Finally, I would like to thank myself for having made this far. Coming to Berkeley is probably the best decision I've ever made. Over the years I have learned, matured a lot and become more resilient. And I knew myself better when exploring many first times.

Thank you for participating this journey and reading until this line. Here's to many more years of bringing new discoveries to the world!

Chapter 1 – Novel waveguide platform for room temperature polaritonics with two-dimensional semiconductors

1.1 Introduction and motivation

Cavity quantum electrodynamics (cavity QED), the control of spontaneous emission of a dipole oscillator has been studied extensively in different systems.[1–5] Confining photons in semiconductor microcavities is of particular interest as the light-matter interaction is strongly enhanced.[6–8] If the coherent energy exchange between the excitonic transition and cavity photon overcomes other damping, the system is said to be in the strong coupling regime. In the strong coupling regime, cavity exciton-polariton systems show strong optical nonlinearities and spontaneous coherence, and they provide a rich variety of polariton physics. The realization of a strong coupling regime in semiconductor microcavities opened a new door to many-body physics inaccessible in other condensate systems[9–12]. Novel macroscopic quantum phenomena, such as non-equilibrium superfluidity[13,14], low-threshold lasing[4,15,16], and Bose−Einstein condensation[1,17–20] , vortex formation[21] have been observed in semiconductor microcavities. The study of strong light-matter interaction in optical cavities have also led to new generation of efficient photonic applications, such as lasing without population inversion[4,16], optical spin switches[22,23], optical logical transistors[24].

Strongly coupling phenomena are often demonstrated at cryogenic temperatures due to small exciton binding energy and strong material disorder in conventional semiconductors.[1,18] The room-temperature coherent mixing can be interesting because such a platform could prompt integrated polariton devices in ambient environment suitable for opto-electronics and strongly correlated phenomena. Recent demonstration of non-equilibrium Bose-Einstein Condensation (BEC) and superfluidity of exciton–polaritons in organic molecules or polymer-filled microcavity at room temperature taking advantage of the processability and flexibility of polymers paves the way for a new generation of opto-electronic devices.[25–27]

The recent discovery of 2D transition-metal dichalcogenides (TMDCs) provides another promising candidate for exciton–polaritons medium.[28–30] TMDCs are van der Waals crystals. When the crystal is thinned down to monolayer thickness, they exhibit absorption coefficients and exciton binding energies two orders of magnitude higher than those of GaAs, suggesting that extraordinary exciton-photon coupling strengths are possible.[31,32] Such a large exciton binding energy and oscillator strength makes the room-temperature exciton-polaritons possible.[33]

Recently, there has been an increasing interest in exploring the strong coupling regime of TMDCs to study strongly correlated phenomena with new limits. Carious cavities, such as distributed Bragg reflectors (DBR) Fabry-Perot cavities[34], Tamm structure[35–37] and plasmonic structures[38,39], can be integrated with TMDCs to form exciton-polaritons in the strongly coupling regime. The selection of appropriate optical cavity involves maximizing the exciton-photon coupling strength while minimizing the losses of the cavity. DBR Fabry-Perot cavities have large mode volumes and typically lead to small Rabi splitting limiting its applications at room temperature (Rabi-splitting measures the splitting between upper-polariton and lower-polariton band, namely, to what extent exciton band and cavity photon mode repel each other). On the other hand, the Tamm and plasmonic structures support small mode volumes, and therefore larger Rabi splitting from 50 to

100meV has been reported at room-temperature[35–37]. However, they both suffer from the absorption loss of metals leading to low quality factors.

Here, we propose and demonstrate the strong coupling regime of WS_2 excitons with photons in a dielectric planar waveguide. The coupling is benefited from small mode volume due to total internal reflection and no metal absorption in the structure. Forming exciton-polaritons with two-dimensional optical waveguides will also enable studies on propagating polaritons and is especially suitable for on-chip polariton circuit applications.[40,41] Studies on waveguide polaritons allow ability to control and direct light at sub-wavelength, which is crucial for nanophotonic devices. Our newly developed waveguide polariton design provides broad opportunities for new physics and device concepts. [42,43]

1.2 Experiment and results

Design and Principle:

Embedding semiconductors in microcavities provide a method to enhance and control the interaction between light and electronic excitations. The most important criterion for the light-matter interaction is the competition between the process of exciton-photon coupling and other relaxation pathways, including both cavity loss and exciton dephasing. In such situations, Fermi's golden rule no longer holds. The Jaynes-Cummings model, which examines a two-level system interacting with a strong near-resonant electric field, can be generalized to describe the strongly coupled excitonic transition and optical cavity mode. In the strong coupling regime, the exact eigenstates of the coupled system are the doublet of the exciton-polaritons which are separated by the Rabi splitting energy, $\hbar\Omega_R$. Rabi splitting measures the coupling strength between excitons and photons and is the critical signature to determine whether the system enters the strong coupling regime.

To achieve large Rabi splitting, cavities with a small mode volume and a high quality factor are required to support these strongly coupled mixed states for such applications as low threshold emission[4,16] and ultrafast switching[24]. The dielectric planar waveguide we proposed confines the photon through total internal reflection and leads to a strongly confined electric field mode profile. The planar waveguide exciton-polaritons system, therefore, produces a large Rabi splitting, indicating strong coupling strength, and could lead to a promising polaritonic platform for discovery of new many-body physics and for integrated opto-electronics applications in the future studies.

Let us start from the general geometry and basic operation principles of the proposed planar waveguide scheme. Figure 1a illustrates the overall device concept of exciton-polariton in a planar waveguide system. The photonics structure we propose for observing exciton-polaritons consists of a prism with high refractive index n_3, a coupling layer with low refractive index n_2, a planar waveguide layer with high refractive index n_1 and a TMDC monolayer on top. (Figure 1a) The refractive indices satisfy $n_1, n_3 > n_2$ and we only focus on oblique angle incidence for which total internal reflection occurs on both n_3- n_2 interface and n_1- n_2 interface. The planar waveguide layer (n_1) works as a cavity to confine light in z dimension and is coupled to the exciton of TMDC monolayer to create exciton-polariton modes. Light can be coupled in the planar waveguide through frustrated total internal reflection at the coupling layer interfaces. The thickness of the

coupling layer can be designed to achieve different cavity quality factor and coupling efficiency.

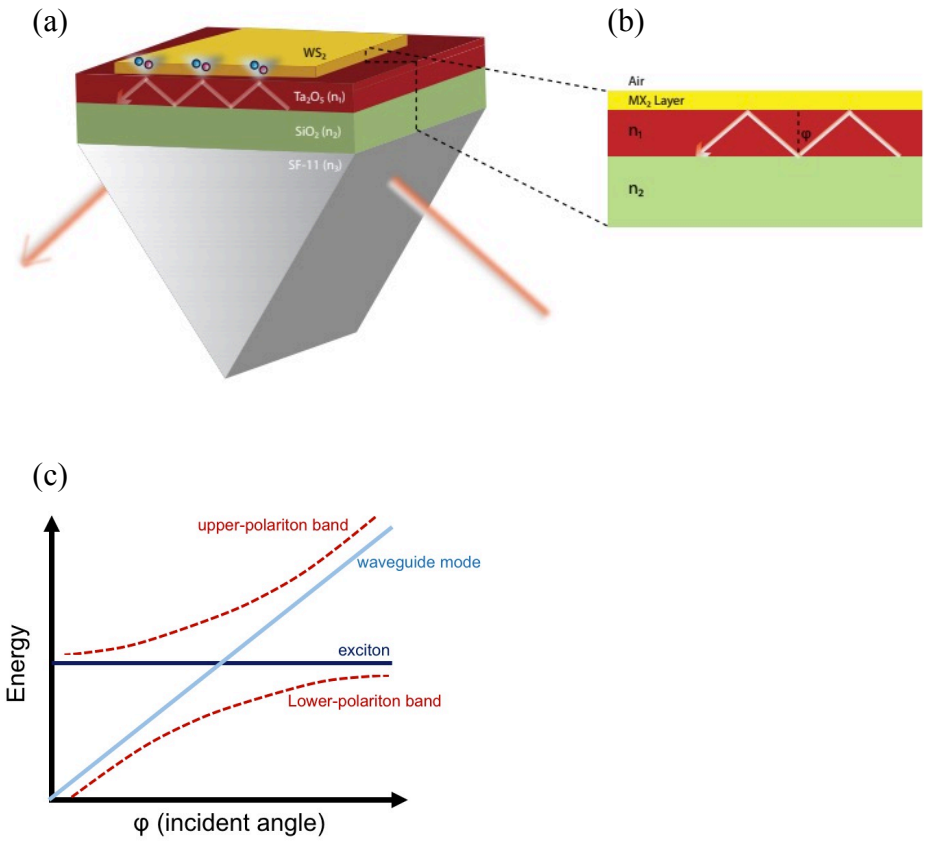

Figure 1: Exciton-polaritons in the designed planar waveguide scheme with TMDC materials. (a) Schematic of our planar waveguide polariton structure. A high refractive index thin film (waveguide layer, red), which is sandwiched between air and a low refractive index film(coupling layer, green), forms a planar waveguide to confine photons in z-direction. Light is coupled in and out via a glass prism (coupling prism, gray) with high refractive index to provide photon momentum required for waveguide resonance. TMDC materials are directly deposited on the top surface of waveguide layer to form coupling between excitons and waveguide modes. (b) The polariton system only considering the planar waveguide and the TMDC film. The ray-optic approach can determine the dispersion of the waveguide resonance in terms of propagation angle φ. (c) Energy dispersion of the upper and lower polaritons. The navy and cyan line show the exciton and waveguide mode energy dispersion. After the coupling is introduced, the upper and lower polaritons becomes the eigenstates of the system (two dashed red lines).

To focus only on the resonance energy without concerning the light coupling method, we can simplify the photonic structure by removing the prism layer and extending the coupling layer to a semi-infinitely thick layer. The simplified model (shown in figure 1b) contains only a planar waveguide and the TMDC monolayer. Following the typical Jaynes-Cummings formalism for exciton-polaritons, we now describe the exciton and waveguide modes by the Hamiltonian with

the rotation wave approximation[8]:

$$H = E_{wg}(\varphi)b^{\dagger}b + E_{ex}c^{\dagger}c + V(b^{\dagger}c + bc^{\dagger}) \qquad (1)$$

where $E_{wg}(\varphi)$ and E_{ex} correspond to the energy levels of the waveguide mode and the exciton transition, which are coupled by the interaction potential $V = \hbar\Omega_R/2$. $b^{\dagger}$, b and $c^{\dagger}$, c are the creation and annihilation operators for photons and excitons, respectively.

The coupled exciton-waveguide system in equation 1 can be represented in terms of exciton and waveguide mode basis as:

$$\begin{bmatrix} E_{wg}(\varphi) & V \\ V & E_{ex} \end{bmatrix} \begin{bmatrix} \alpha \\ \beta \end{bmatrix} = E_{pol}^{\pm}(\varphi) \begin{bmatrix} \alpha \\ \beta \end{bmatrix} \qquad (2)$$

The eigenstates of the equation represent superposition of the bare states, which are called polaritons. The eigenvalue $E_{pol}^{+}(\varphi)$ and $E_{pol}^{-}(\varphi)$ correspond to the angle-dependent hybrid eigen-energies of the upper and lower polariton branches. The mixing coefficients $|\alpha|^2$ and $|\beta|^2$ describe the relative photonic and excitonic content of the polaritonic states, and α, β are known as the Hopfield coefficients. The full expression of $E_{pol}^{\pm}(\varphi)$ can be further written as:

$$E_{pol}^{\pm}(\theta) = \frac{E_{wg}+E_{ex}}{2} \pm \sqrt{(\frac{E_{wg}-E_{ex}}{2})^2 + V^2} \qquad (3)$$

In the special case of zero detuning, i.e. $E_{wg} = E_{ex}$, the energies of polaritons $E_{pol}^{\pm} = E_{ex} \pm V = E_{ex} \pm \hbar\Omega_R/2$, indicating that the upper and lower polariton are split by $\hbar\Omega_R$ which is the so-called Rabi splitting.

The waveguide resonance energy E_{wg} is a function of the propogating angle φ due to the energy-momentum dispersion of the planar waveguide. The full analysis of the optical modes in the planar waveguide is well-known[44] and will be described later in the simulation section. Here, we use the ray-optic approach to provide a simple understanding of the dispersion of a planar waveguide. Shown in figure 1b, the light propagating in the z direction is considered to be composed of plane waves moving in zig-zag paths in the x-z plane undergoing total internal reflection at the interfaces bounding the waveguide. The resonance optical mode requires constructive interference as the waves travel through the guide, so the total phase change for a point on a wavefront that travels from the n_1–n_2 interface to the n_1–air interface and back again must be a multiple of 2π. This leads to the following condition,

$$\frac{2E_{wg}(\theta)d}{c}\sin\theta - 2\phi_{1-2} - 2\phi_{1-air} = 2m\pi \qquad (4)$$

where n, d is the refractive index and thickness of the waveguide, θ is the angle of reflection with respect to the z direction, as shown in Figure 1b, m is the mode number, and $\phi_{1\text{-}2}$ and $\phi_{1\text{-air}}$, are the phase changes suffered upon total internal reflection at the interfaces. In this thesis, we choose to focus only on the fundamental TE mode (m=0, polarization in y-direction) of the planar waveguide since this mode confines the electric field the tightest and generates the largest coupling strength.

Solving equation 4 gives the waveguide resonance energy $E_{wg}(\varphi)$ as a function of φ and typically results in a dispersion relation shown as red curve in figure 1c.

As we place a monolayer TMDC on top of the planar waveguide, the uncoupled exciton mode (shown as navy line in figure 1c) and the uncoupled waveguide mode (shown as cyan line in figure 1c) start to mix due to the coupling potential V. After diagonalizing equation 2, we plot the angle-dependent eigen-energies of the upper and lower polaritons shown as the dashed red curves in the figure 1c, assuming that the coupling potential is independent of φ. The planar waveguide design allows us to achieve largest Rabi splitting at zero detuning condition insensitive to the fabrication error.

To optimize the Rabi splitting, a quantitative understanding of the coupling potential V is needed. In our model, the coupling potential V should relate to mode volume and oscillator strength through the following expression:

$$2V = \hbar\Omega_{\mathrm{R}} = \sqrt{\frac{(\hbar e)^2}{2\varepsilon m_0 L_{eff}} f} \quad (5)$$

where ε is the permittivity, L_{eff} is the effective length of the planar waveguide, and f is the oscillator strength of a single layer TMDC. The effective length of a planar waveguide is expressed as $L_{eff} = \frac{\int \varepsilon {E_y}^2 dx}{\varepsilon E_y^2(x_0)}$ for the zero-order TE mode, where x_0 is where the TMDC layer is. It is now clear to see the advantage of using a planar waveguide over the distributed bragg reflector mirrors as a cavity in terms of larger Rabi splittings. The effective length of distributed bragg reflector mirrors is typically much larger than the real cavity distance due to the electric fields distributed in the first few layers of dielectric. The effective length of a planar waveguide, however, is only of the order of half wavelength since the field decay outside of waveguide layer is evanescent. This is a direct consequence of the fact that the photon confinement in waveguides is through total internal reflections.

To estimate the Rabi splitting, we take the simulated value of $L_{eff} = 90nm$ from an optimized structure shown in figure 3a and the experimental value of f = $8\times10^{17}/m^2$ from the A-exciton absorption of a WS_2 monolayer from chemical vapor deposition (CVD). The details of the methods to acquire these numbers is described in the simulation section. We can also verify that the coupled system is indeed in the strong coupling regime by comparing the Rabi splitting $\hbar\Omega_{\mathrm{R}}$ with γ and κ, where γ and κ are the homogeneous decay rates of the matter polarization and the light in the cavity, respectively[45]. The homogeneous linewidth ħγ of A-exciton in TMDC monolayer at room temperature is typically ~25meV from previous literatures[46] while the cavity linewidth ħκ in our simulation is around ~10meV. Therefore, the condition for strong coupling regime $\hbar\Omega_{\mathrm{R}} > \hbar\gamma, \hbar\kappa$ is satisfied.

When the whole stacked layers is considered, the energies of polariton modes are not perturbed significantly since the optical modes decay evanescently in the coupling layer. The coupling layer is chosen to be thick enough such that the mode tail in the prism layer is negligible. Thus, the model describing only coupling between excitons and waveguide modes is still valid. However, the coupling efficiency from a free space photon to cavity photon and the quality factor of the

waveguide depend on the thickness of the coupling layer and we will address these issues in the simulation section.

Simulation:

Transfer matrix method (TMM) is used to simulate the reflection spectrum of the WS_2-planar waveguides system to optimize waveguide parameters to achieve the largest Rabi splitting and the best coupling efficiency. In the TMM simulation, we include the measured TMDC monolayer optical properties and realistic material parameters. The simulated reflection spectrum can be compared with both theory and experiments and enable us to optimize the photonic structure for enhancing light-matter interactions. Here, we choose the active medium to be a WS_2 monolayer as an example.

To acquire the accurate optical properties of WS_2 monolayer for simulation, reflection spectroscopy is performed. Figure 2a shows the measured reflection spectrum from a transferred CVD WS_2 monolayer on a sapphire substrate. Two main peak features at 2.0eV and 2.4eV arise from the absorption of A-exciton and B-exciton transitions of WS_2, respectively. From the measured reflection spectrum, we can deduce the absorption spectrum and the permittivity of the free-standing WS_2 (shown in Figure 2b). The thicknesses of the WS_2 monolayer is assumed to be 0.649nm. The extracted absorption spectrum of the WS_2 reaches 20% at the A-exciton resonance and this value is surprisingly large compared to exciton absorption of traditional semiconductors.[47,48]

The permittivity spectrum of the WS_2 monolayer is fitted by a multi-Lorentzian model. The peaks and dispersion in imaginary and real parts of permittivity are represented by multiple resonances as

$$\varepsilon = \varepsilon_\infty + \sum_i \frac{f_i E_{0,i}^2}{E_{0,i}^2 - E^2 + i(\hbar\gamma_i)E} \qquad (6)$$

where E the photon energy, ε_∞ the background dielectric contribution, f_i the oscillator strength, $E_{0,i}$ the resonance energy, and $\hbar\gamma_i$ the broadening of resonance i. From the fitting, the E_0, f and $\hbar\gamma_i$ for the A-exciton resonance is determined to be 2.0 eV, $8\times10^{17}/m^2$ and 60meV, respectively. These values are used in the simulation and the coupled oscillator model estimation. The relatively broad exciton linewidth in CVD WS_2 mostly originates from inhomogeneous broadening due to growth defects and can be improved by better sample quality.

To optimize the planar waveguide structure, we perform a simulation based on the transfer-matrix formalism to deal with multilayer reflection problems. The custom simulation is written in Python and allow us to explore materials, dimensions, tolerances, and coupling conditions to provide theoretical bounds on coupling efficiency and Rabi splitting. These simulated parameters included polarization and incident angle of the light beam, the TMDC's optical properties in various temperature conditions, and the structure of planar waveguide layers. Drawing upon these results we found the optimal parameters, compatible with standard fabrication techniques, for the coupling efficiency, quality factors, and Rabi splitting.

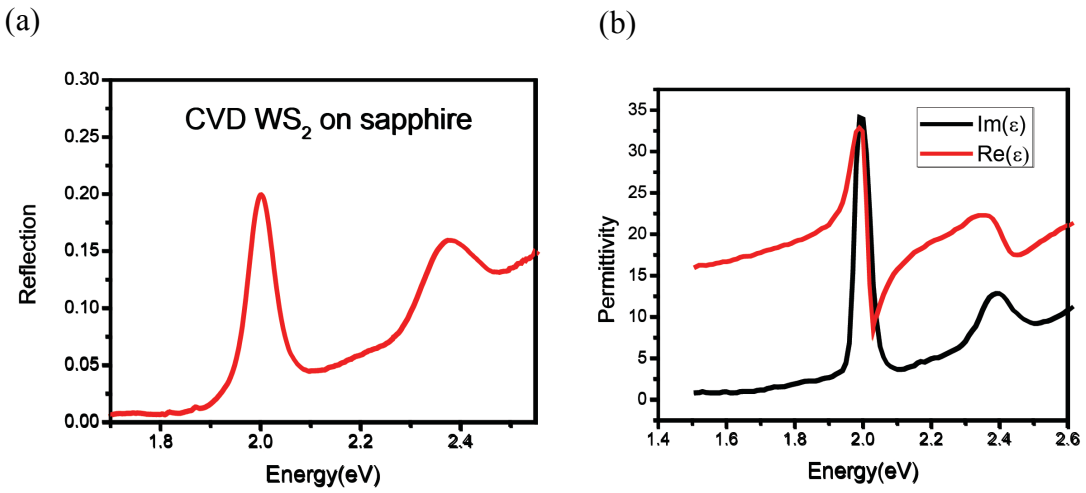

Figure 2: Measured optical properties of chemical-vapor-deposition (CVD) WS_2 monolayer. (a) Experimental reflection contrast spectrum of a transferred CVD WS_2 monolayer on a sapphire substrate. The reflection contrast of a WS_2 monolayer reaches 20%, which indicates a much larger oscillator strength compared with conventional semiconductor quantum wells. (b) Extracted permittivity of a WS_2 monolayer from the experimental data in (a).

A schematic of the optimized structure used is shown in Figure 3a. The dielectric multilayer consists of infinitely thick glass SF-11(n=1.743, thickness 60nm), a coupling layer of SiO_2 (n = 1.444, thickness 500nm), a waveguide layer of Ta_2O_5 (n = 2.0856, thickness of a WS_2 monolayer). The thin layer of Ta_2O_5 forms a high refractive index waveguide layer and confines electric fields in a small mode volume which is of the order of the waveguide thickness, as opposed to DBR mirrors which have mode volume of many dielectric layers. The SF-11 glass layer has a high refractive index compared to the SiO_2 coupling layer and therefore supports total internal reflection at the interface when the coupling angle θ is larger than the critical angle $\theta_c = \sin^{-1}(n_2/n_3)$. In this regime, light can only evanescently couple in and out from the planar waveguide and maintain a relatively high Q cavity.

The simulated reflectance for different incident angles and wavelengths without the TMDC monolayer is shown in figure 3b. The optimized thickness of SiO_2 and Ta_2O_5 layers are 500nm and 60nm which is used as the experimental conditions later. The polarization is set in the TE mode direction for simplicity. A small absorption in Ta_2O_5 layer is artificially introduced to make the waveguide mode visible. Without the TMDC monolayer, a clear zero-order TE cavity mode is observed. While the incident angle θ of reflection spectrum can be related to $K_{//}$ (K parallel), the energy dispersion of the TE cavity mode in terms of incident angle θ, which relates to propagation angle φ through Snell's law, follows the typical planar waveguide resonance equation (equation 3). The quality factor of the cavity mode is determined by the intrinsic absorption of the dielectric waveguide as well as the coupling layer thickness.

The simulated reflectance in figure 3c includes a WS_2 monolayer on top of Ta_2O_5 waveguide and the other parameters are kept the same as the previous simulation. The optical parameters of the WS_2 monolayer are taken from the measured CVD WS_2 monolayer shown in the figure 2b. When a monolayer of WS_2 is introduced, clear anti-crossing behavior occurs at the crossing point of A-exciton resonance and waveguide mode, indicating that a strong coupling between WS_2 monolayer and Ta_2O_5 planar waveguide is formed. The Rabi splitting achieved in the optimized waveguide structure is 102meV which is much larger than the room temperature thermal energy ~ 25meV. The simulation is conducted as following condition: infinite thickness of air, 0.649nm of WS_2, 60nm of Ta_2O_5, 500nm of SiO_2, infinite thickness of SF-11.

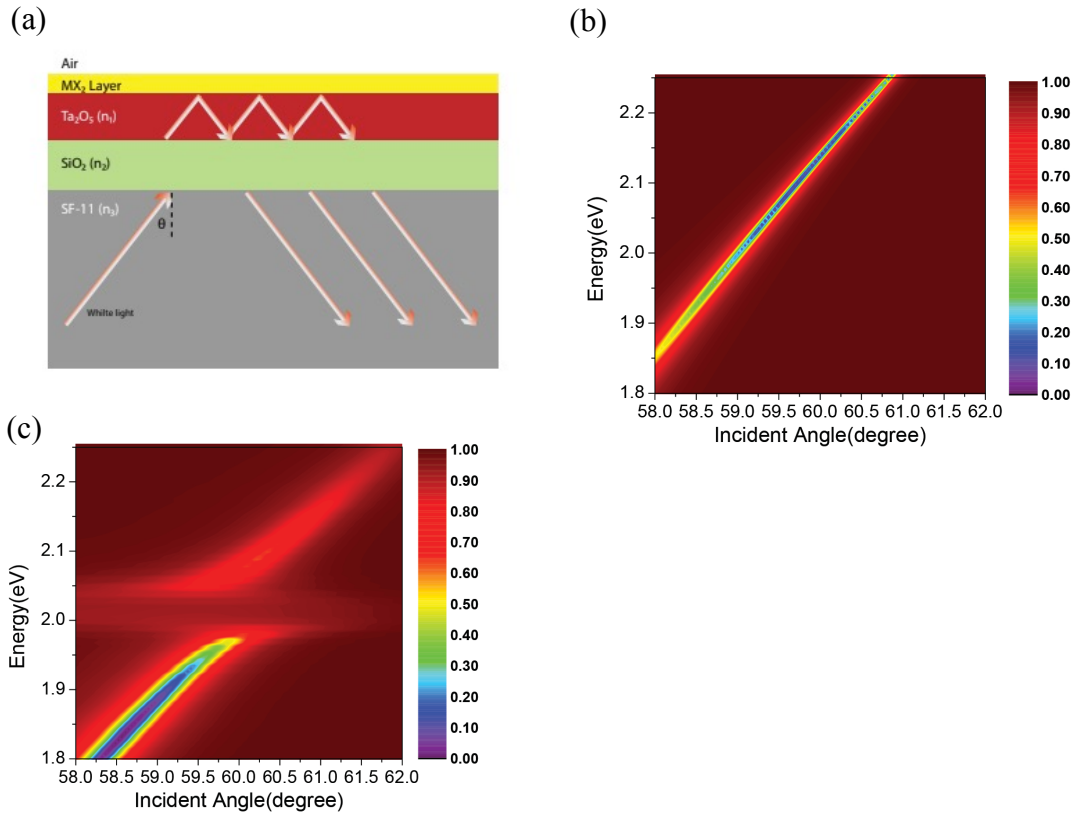

Figure 3: Transfer-matrix-method (TMM) simulation of a coupled exciton-waveguide system. (a) An optimized waveguide structure is used in the TMM simulation. The dielectric multilayer consists of infinitely thick glass SF-11(n=1.743), a coupling layer of SiO_2 (n=1.444), a waveguide layer of Ta_2O_5 (n=2.0856), a WS_2 monolayer, and an infinitely thick layer of air(n=1). The incident angle θ, related to the propagation angle φ through Snell's law, is set to be large than all relevant critical angles, therefore the electric field is evanescent in the SiO_2 coupling layer and propagating in both Ta_2O_5 waveguide layer and glass SF-11 layer. (b) The contour plot shows the angle-dependent reflectivity from the planar waveguide without TMDC monolayer. The dip in the reflectivity map out the dispersion of the planar waveguide. (c) The angle-dependent reflectivity from the planar waveguide with a TMDC monolayer simulated with experimentally-derived parameters. The low reflectivity points map out the dispersion of the upper and low polaritons.

Angle-resolved reflection spectra

To experimentally investigate the strong coupling between TMDC monolayer and a planar waveguide resonator, we prepare an equilateral SF-11 glass prism coated with 500nm SiO_2 coupling layer followed by a 60nm Ta_2O_5 layer, forming a high refractive index waveguide. The high refractive index prism and a 500nm coupling layer of SiO_2 are used to evanescently couple light in and out of the planar waveguide. The two-dimensional waveguide creates an extremely small optical mode volume, which is largely confined within in the 60nm-thick Ta_2O_5 layer[34,49]. A large-area continuous WS_2 film is grown by CVD method on a silicon dioxide surface, and we use a wet-transfer method to transfer it to the Ta_2O_5 surface (see method for detail information).

Figure 4a shows our experimental data from angle-resolved reflection spectroscopy for TE polarization on a WS_2 exciton-polariton device based on the planar waveguide. The detailed method is described in the method section Reflection and Photoluminescence Measurements. The reflection is nearly unity due to total internal reflection except when the lights coupled to an optically bright mode. The reflection spectral minima map the position of the upper and lower polariton modes and show a clear anticrossing behavior at the A-exciton energy and 58.5° incident angle.

Figure 4b shows several vertical linecuts of the contour plot in figure 4a to further investigate the evolution of the lower and upper polaritons. The black and red circles mark the spectral minima on each spectrum, indicating the energy of lower and upper polaritons at a specific incident angle. Starting from θ=57.0°, at which the waveguide mode is red-detuned from the exciton energy, the waveguide and exciton mode are separated and no apparent shift on both modes. As the incident angle approaches θ=58.5°, the waveguide resonance gets closer to the exciton energy. The coupling potential between waveguide and exciton modes make it impossible to describe the system by either waveguide nor exciton modes. Instead, the normal modes of the system can only be explained as lower and upper polaritons; instead the linear superposition of waveguide and exciton modes must be considered. These two modes repel each other in the vicinity of θ=58.5°, corresponding to the zero detuning condition. As θ increases further, the waveguide mode starts to blue-detune from the exciton energy and the mixing between them becomes smaller. Therefore, the resonances can be described by the waveguide and exciton modes again.

The spectra at different angles are fit with two lorenzian functions and the extracted energies and linewidths of the lower and upper polaritons are plotted in figure 4c. The resonance energies for lower and upper polaritons show an anticrossing behavior as expected. We fit the energy of the two peaks as a function of incident angle using the coupled oscillator model described in equation 2 and 3. When we convert the Energy-theta (θ) plot to Energy-k plot (since our incident angle is large that $k_{//}$ which is a function of the photon wavelength), the Rabi splitting becomes ~30meV. The extracted upper and lower polariton branches are shown in figure 4c as dashed red and black line.

We observe well-separated upper and lower exciton-polariton resonances and a large exciton-polariton Rabi splitting of 30 meV at room temperature.

Angle-resolved photoluminescence spectra

Figure 5a shows the experimental data from angle-resolved photoluminescence (PL) spectroscopy on the WS_2 exciton-polariton device excited with 532 nm continuous wave laser. The extracted lower and upper polariton dispersions obtained in figure 4c are also shown as white and gray dash curves in the same plot for comparison. Figure 5b shows the line plots of PL spectra at different incident angles for clarity. The detailed method is described in the method section Reflection and Photoluminescence Measurements.

The observed PL spectrum shows dominant emission from the lower polariton branch while the emission from the upper polariton branch is not detected. Note that the angle-resolved emission follows the dispersion of lower polariton. In the PL measurement, the exciton-polariton states is populated through scattering of the non-resonantly pumped excitons. The fact that only the PL from lower polariton branch is observed indicates efficient energy relaxation of exciton-polaritons in the strong coupling regime with the planar waveguide structure.

The PL also shows a long tail down to 1.8eV which is also observed in previous studies with Fabry-Perot cavities.[35,37] The reason for this PL tail is could be explained by enhanced PL from WS_2 defect states due to waveguide Purcell effect[50] or polariton parametric amplification scattering into the waveguide modes[51]. An angle-resolved power-dependent PL measurement with clean TMDC materials would be desired to distinguish these two effects.

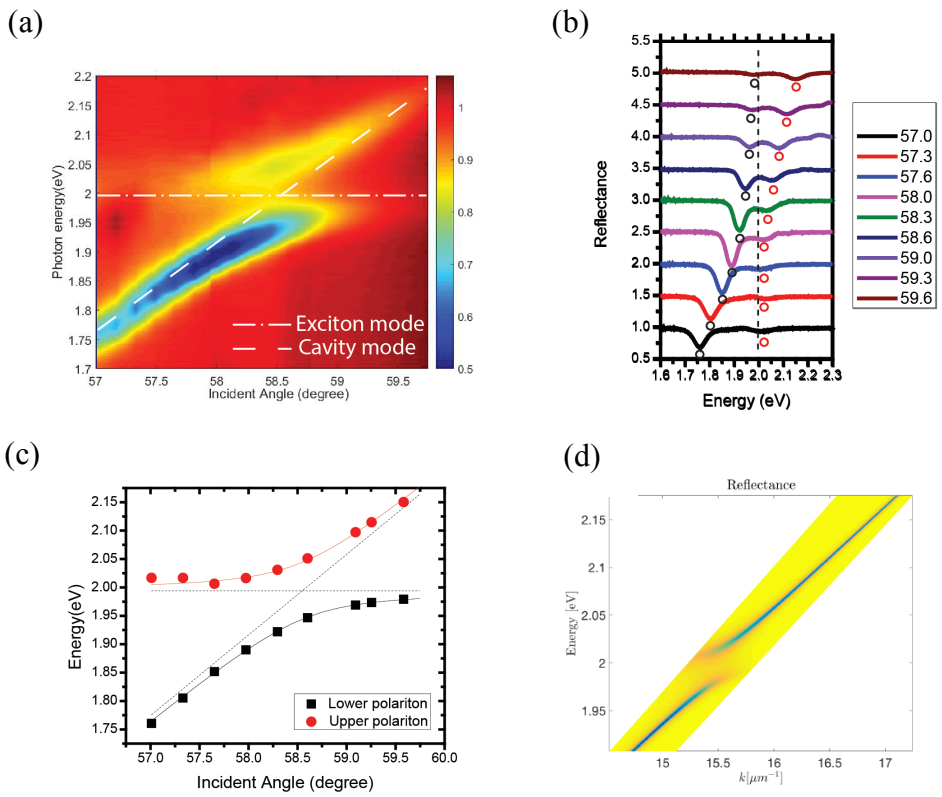

Figure 4: Observation of Rabi splitting in experimental angle-resolved reflection spectra. (a) Contour plot of the experimental angle-resolved reflection spectra. The dispersion of upper and lower polaritons show clear anti-crossing behavior, evidencing that our coupled system is well situated in the strong coupling regime. The white dash and dotted lines indicate the un-coupled cavity and exciton modes, respectively. (b) Line plots of reflection spectra at different incident angles. Each spectrum is offset by a fix amount. The black and red open circles mark where the lower and upper polariton energies are, respectively. (c) The measured lower (black dots) and upper(red dots) polariton energies. The fitting using a simple Jaynes-Cummings model is shown with red and black dash curves. (d) After convert Energy-theta (θ) plot to Energy-k plot (since our incident angle is large that $k_{//}$ which is a function of the photon wavelength), the Rabi splitting becomes ~30meV.

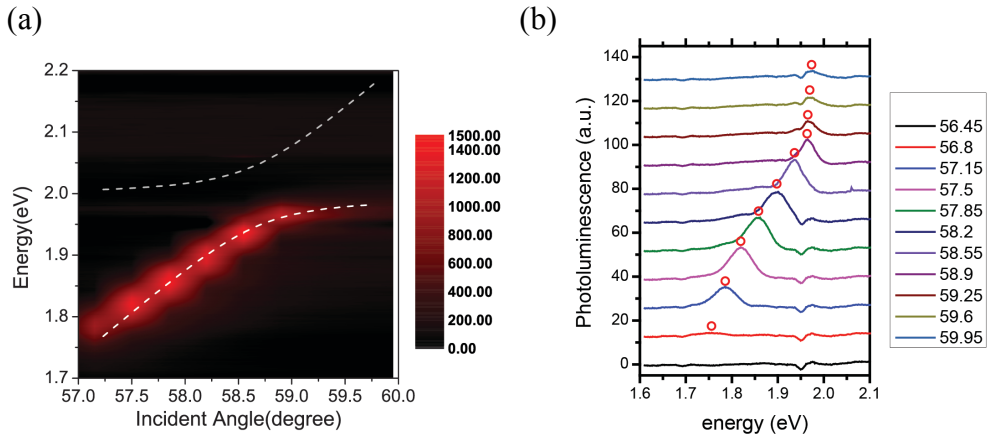

Figure 5: Experimental angle-resolved photoluminescence (PL) spectra. (a) A contour plot of the experimental angle-resolved PL spectra. The white and gray dash curves are the same fitting obtained from figure 4c. The PL shows a long tail down to 1.8eV which might be explained by enhanced PL from WS_2 defect states due to waveguide Purcell effect. (b) Linecutsof reflection spectra at different incident angles. Each spectrum is offset by a fix amount. The red open circles mark the lower polariton energy at each incident angle θ.

1.3 Methods and Experimental setup

Fabrication of planar waveguide

The optical properties of the planar waveguide is simulated with transfer-matrix-method software. The software also simulates the coupling between monolayer TMDC and the planar waveguide. Once the optimal structure is found, we purchase the glass SF-11 prisms from Edmund optics. The SiO_2 and Ta_2O_5 layers are made using customized coating service from Edmund optics.

Synthesis and transfer of WS2

The WS_2 growth on SiO_2/Si wafer is done using the metal−organic chemical-vapor-deposition(CVD) method. The chemical precursors for tungsten and sulfur atoms are tungsten hexacarbonyl ($W(CO)_6$, THC, Sigma-Aldrich 472956) and diethyl sulfide ($C_4H_{10}S$, DES, Sigma-Aldrich 107247) , respectively. The growth was performed under a temperature of 500 °C and growth time of 30 hours. More detailed information can be found in reference[52].

The grown CVD WS_2 monolayer on SiO_2 is then coated with Poly(methyl methacrylate)(PMMA) for support and let dry in ambient condition. The supported CVD WS_2 monolayer can be easily peeled off from the substrate when submerged into water with an oblique angle. The prism with

planar waveguide prepared is used to fish up the PMMA-supported WS_2 floating on the water. The PMMA is later dissolved in acetone solution.

Reflection and Photoluminescence measurements

For angle-resolved reflection spectroscopy, a supercontinuum laser (Fianium, WL-SC-400-15) containing photon wavelength from 450nm to 800nm is expanded to a 1cm diameter beam size through a telescope. A Glan-laser calcite polarizer is used to set the polarization to align with TE mode of the planar waveguide. The laser beam is focused onto the planar waveguide plane through one side of the prism using an air-spaced achromatic doublet lens with f=15cm. The incident angle is controlled by a movable slit with 500μm width to provide desired angular resolution. The incident angle can be measured by the reflected light from the prism side. The reflected light from the planar waveguide is then collected on the other side of the prism and sent into a spectrometer for analysis.

For angle-resolved photoluminescence spectroscopy, a 532nm continuous wave laser is used for pumping at the normal direction of the planar waveguide. The collection angle is controlled by a movable slit with 500μm width, whose position is determined previously by the reflection measurement. The emission from WS_2 through the prism side is then sent into a spectrometer for measurements.

1.4 Summary and Future outlook

In summary, we present a simple and innovative method to strongly couple two-dimensional materials with dielectric planar waveguides. The new method has several advantages: (1) all photonic elements are made of dielectric materials avoiding metal absorption in contrast to plasmonic designs. (2) The light confinement is based on total internal reflection leading to a small mode volume compared to distributed bragg reflecting mirrors. (3) The surface of two-dimensional material is exposed and can be easily accessed for device fabrication in the future.

By transferring WS_2 monolayer onto designed planar waveguides, we demonstrate that the waveguide mode and the A-exciton mode of monolayer WS_2 can reach a strong coupling regime by analyzing the angle-resolved reflection spectra. Due to the small mode volume of the planar waveguides, a strong coupling potential is expected. A large Rabi splitting of 100meV is observed experimentally. The experimental data is also well described by both Jaynes-Cummings model and the transfer-matrix-method simulation. The angle-resolved photoluminescence surprisingly shows a long tail in the low energy side of spectrum which might be caused by defective states or polariton parametric amplification. The large Rabi splitting and flexible design in the quality factor permit a promising platform for future exciton-polariton studies with two-dimensional materials.

Chapter 2 – High speed photodetector using 2D Black Phosphorous

2.1 Introduction and motivation

2D layered materials are one of the major developments in materials science for the past decade, and many fruitful physics and possible application emerged afterwards. Among them, black phosphorene (BP) is a material with extremely high mobility[53]. Combining this nature with its electrical gate tunable bandgap and optical transition, applying phosphorene as a high speed photodetector seems to be a feasible idea. Many different detector structures and materials are developed to cover a large range of applications. Most typical photodetectors in visible and infrared use silicon and germanium for wavelengths from 0.4 to 1.0 μm and at longer wavelengths up to 1.8 μm.[54,55] However, they both have indirect bandgaps at these wavelengths, which result in relatively small bandwidth-efficiency products. Consequently, for high-speed applications, direct bandgap semiconductors which have strong absorption in the infrared range are desired.

Recently our group has demonstrated that the bandgaps of monolayer, bilayer, trilayer phosphorene are 1.73, 1.15, and 0.83 eV, respectively[56], and bulk black phosphorus has a bandgap of 0.35 eV. In particular, the band gap of bilayer and trilayer phosphorene (at 1.15 and 0.83 eV) matches well with the silicon bandgap (1.1 eV) and telecom photon energy (0.8 eV), respectively[56].

Because black phosphorene is a layered Van der Waals material, one can construct atomically-thin vertical junctions through scotch tape exfoliation and pickup transfer methods.[57] The atomically-thin junction distances reduce the electron transit time and yield high-speed optical detection. A traditional design is a lateral source and drain structure, where photo-excited electrons have to travel through several micrometers, and can be scattered and delay the response time. Here we designed a vertical electrode structure for our photodetector that can shorten the path electrons travel and thus enhance the response time.

2.2 Experiments setup and sample preparation

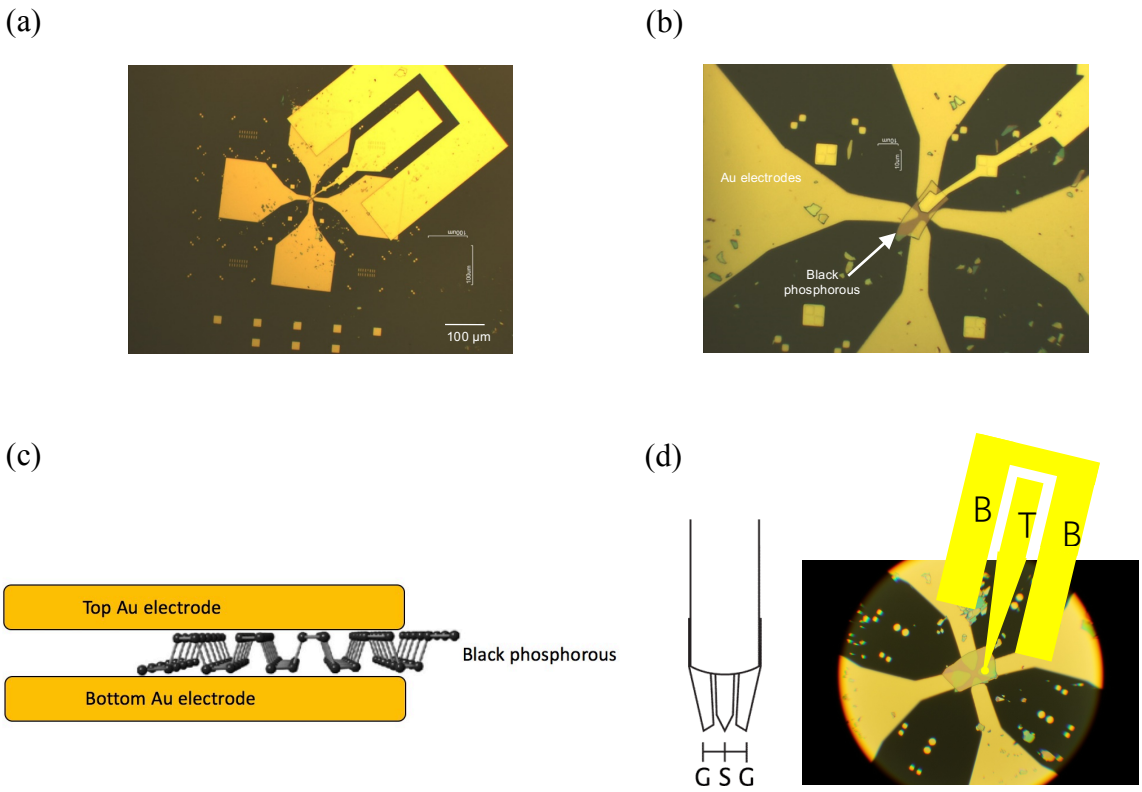

Fig. 6: A schematics of our designed structure. (a) and (b) show a top view of our vertical structure, viewed through a microscope (c) is a schematic of the side view of the device. Black phosphorous is sandwiched between top and bottom Au electrodes. This vertical design shortens the electron travel distance compared with traditional lateral source and drain design. (d) The bottom and top electrodes are then connected with a G-S-G high speed probe for the AC signal measurements.

Fig. 6 shows the our black phosphorous device and the high-speed probe used to measure the signal. A high speed Ground-Source-Ground (G-S-G) RF probe is connected with deposited B-T-B (Bottom-Top-Bottom) to detect the photocurrent signal.

A super-continuum laser (YSL Photonics SC-Pro, wavelength 430nm-2400nm) or a SCG 800 supercontinuum fiber (Newport) pulsed laser (wavelength from 450nm-1500nm), is used to excite electron-hole pair and turn them into photocurrent. A real time measurement set-up (fig. 7) is employed to record the photocurrent (photo-voltage). A small bias (can be changed accordingly with the series resistor) is applied across two electrodes to create electric field to separate electron and holes and create photocurrent.

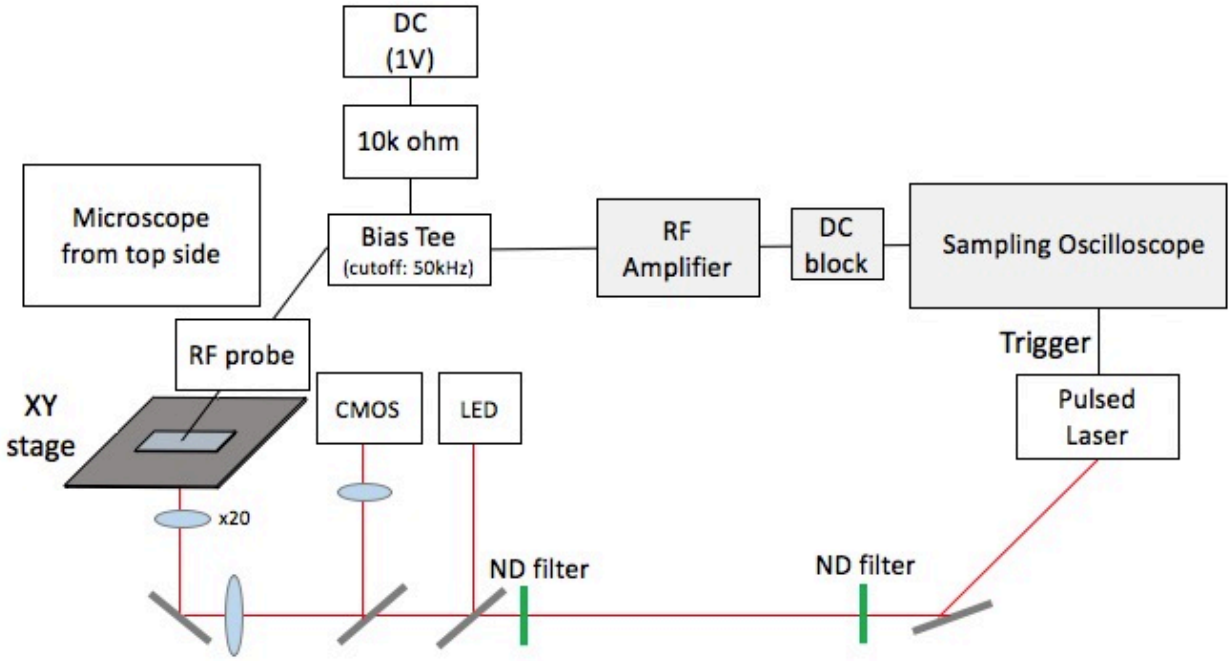

Fig. 7 Measurement setup. While the sample is suspended on the XY stage, we shine laser pulse from the bottom electrodes (which is Au electrode, and Au electrode will couple certain portion of light into black phosphorous) and adjust the setup using an optical microscope from the top side to make sure the light would excite at the black phosphorous and electrode junction.

2.3 Experimental Results

Power dependence and electrical resistance of the photodetector

Here we use a lock-in amplifier to test the input power dependence and efficiency of our photodetector devices. The measured photovoltage shows a linear relation to power for power 0uw all the way to 6.5uw (estimated power couple into BP from bottom Au electrode). A **SC-Pro supercontinuum laser** (single pulse width 100 ps, 4MHz repetition rate, wavelength ranging from 400nm-2400nm) is used for the measurement. The responsivity is 96 μV/μW. The power is estimated as that when light is shined on the Au electrode and only~1% of energy is coupled into black phosphorous.

We have also measured the resistance of the BP sample, which is estimated to be 270ohm.

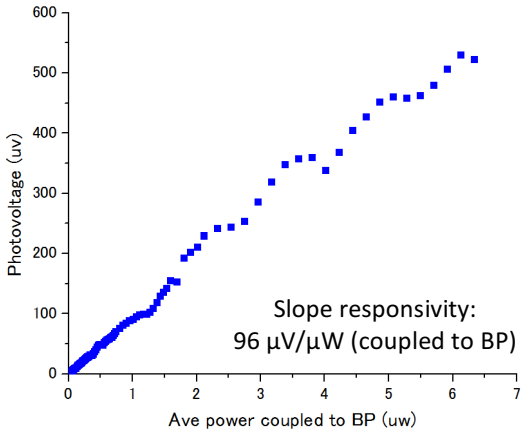

Fig. 8 Power dependence of our black phosphorous device. X-axis shows the estimated light power being coupled into BP sample. Y-axis shows a photo-voltage measured by lock-in amplifier.

Real time photo-response of the photodetector---with SC Pro supercontinuum laser and Tektronix CSA 803C oscilloscope

Following is the real-time photocurrent(photo-voltage) measurement by supercontinuum laser (single pulse width 100ps, 4MHz repetition rate, wavelength ranging from 400nm-2400nm) with different input power. The single pulse has a 100ps width in the time domain, and the photo-voltage signal we measured from oscilloscope has a FWHM around 200ps. The measurement is done with a RF amplifier (MITEQ, AMF-4D-30M-8G-20-13P 0.03–8 gain 30dB, bandwidth 0.03-8GHz) and K-cable. The broadening may be coming from reflection and noise in the RF amplifier, cable and connector or the devices itself, for this we haven't been able to de-couple at this time,. A small bias (1V when series with a 10k ohm resistor, this voltage and resistor can be changed accordingly) is applied across two electrodes to create electric field to separate electron and holes and create photocurrent.

(a)

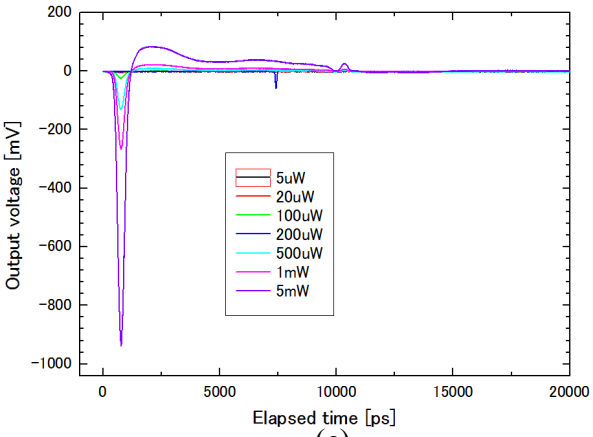

(b)

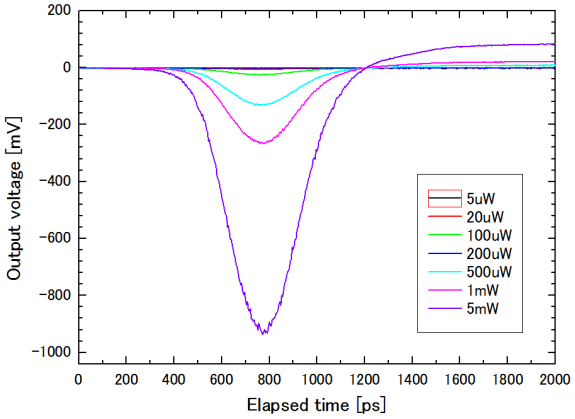

(c)

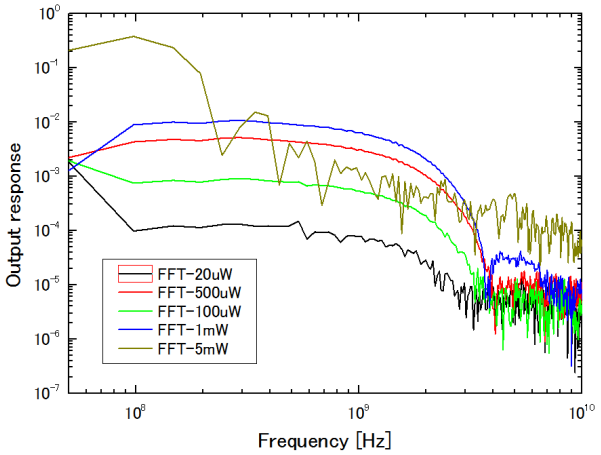

Fig. 9 Photo-voltage measurement (with a RF amplifier) in time domain (a) and (b) BP photodetector reveals a 200ps FWHM. (a) and (b) are the same plot while (b) is a zoom-in of (a). (a) (c) is a plot showing output (b) (photo-voltage) response versus frequency.

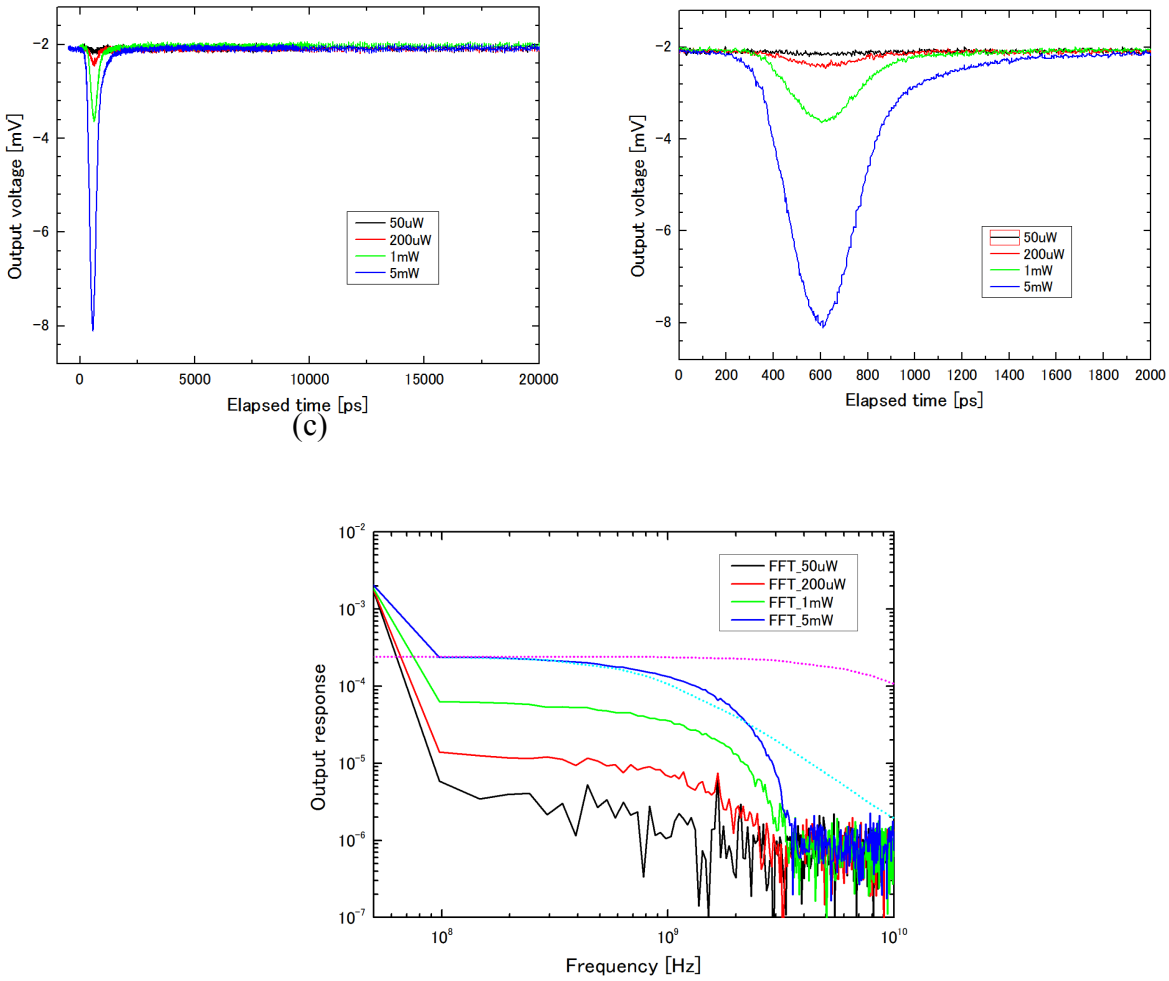

Fig. 10 Photo-voltage measurement in time domain (without RF amplifier) (a) and (b) BP photodetector reveals a 200 ps FWHM. (a) and (b) are the same plot while (b) is a zoom-in of (a). (c) is a plot showing output (photo-voltage) response versus frequency. The response time is roughly the same while the noise has been significantly reduced.

Real time photo-response of the photodetector---SCG800 supercontinuum fiber (NewPort) laser with Agilent 86100A sampling oscilloscope.

A laser with shorter pulse width is exploited to study the limitation of our scheme. Here we employed a SCG800 laser, Agilent 86100A sampling oscilloscope to measure the photo-voltage. The SCG-800 Supercontinuum Fiber Device is a supercontinuum generation device for use with 800 nm femtosecond lasers (that has a 82MHz repetition rate), and after the fiber it can generate 450nm~1500nm in wavelength, single pulse width is ~150fs. We put a 500 short-pass filter so only the 450nm~500nm light would pass and couple into the black phosphorous.

Comparing with previous Tektronix CSA 803C oscilloscope, the Agilent 86100A sampling oscilloscope has a bandwidth that can go up to 50GHz (AC), and ideally can resolve much faster response time.

One can observe the much faster response in this scheme, shown in fig. 11 (a) and (b), with a peak that has ~36ps FWHM. While (a) is measured without the amplifier. The noise is significantly reduced without amplifier.

(a)

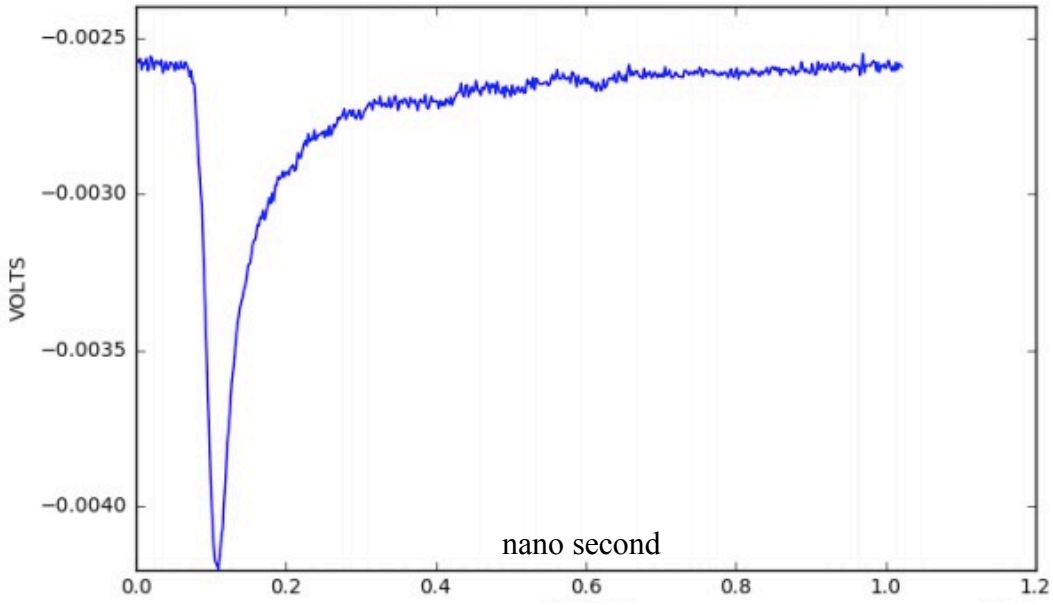

Fig. 11 Time domain response of BP photodetector excited with pulse laser (82MHz repetition rate). (a) is the photo-voltage measured without the RF amplifier, and with the 0.2 mW laser power.

2.4 Summary and Future outlook

We have achieve a high-speed photodetector made of black phosphorene with a bandwidth up to 10GHz. At the same time, the direct bandgap of black phosphorene provides large optical absorption and results in large photo-responsitivity. The simplicity of the vertical structure also allows us to integrate with optical waveguide for telecommunication purpose. A silicon waveguide provides easy access for optical excitations, enhancing the responsitivity and paves the way for future on-chip integration for telecommunication applications. These ultrafast photo-detectors based on phosphorene can be integrated either with silicon photonics or on a flexible substrate, which can open up exciting new application capabilities.

REFERENCES

1. Kasprzak, J. *et al.* Bose-Einstein condensation of exciton polaritons. *Nature* **443,** 409–414 (2006).
2. Weihs, G. *et al.* Exciton–polariton lasing in a microcavity. *Semicond. Sci. Technol.* **18,** S386 (2003).
3. Huang, R. *et al.* Exciton-polariton lasing and amplification based on exciton-exciton scattering in CdTe microcavity quantum wells. *Phys Rev B* **65,** 165314 (2002).
4. Deng, H., Weihs, G., Snoke, D., Bloch, J. & Yamamoto, Y. Polariton lasing vs. photon lasing in a semiconductor microcavity. *Proc. Natl. Acad. Sci.* **100,** 15318–15323 (2003).
5. Byrnes, T., Kim, N. Y. & Yamamoto, Y. Exciton-polariton condensates. *Nat Phys* **10,** 803–813 (2014).
6. Walther, H., Varcoe, B. T. H., Englert, B.-G. & Becker, T. Cavity quantum electrodynamics. *Rep. Prog. Phys.* **69,** 1325 (2006).
7. Miller, R. *et al.* Trapped atoms in cavity QED: coupling quantized light and matter. *J. Phys. B At. Mol. Opt. Phys.* **38,** S551 (2005).
8. Khitrova, G., Gibbs, H. M., Kira, M., Koch, S. W. & Scherer, A. Vacuum Rabi splitting in semiconductors. *Nat Phys* **2,** 81–90 (2006).
9. Anderson, M. H., Ensher, J. R., Matthews, M. R., Wieman, C. E. & Cornell, E. A. Observation of Bose-Einstein Condensation in a Dilute Atomic Vapor. *Science* **269,** 198 (1995).
10. Bradley, C. C., Sackett, C. A., Tollett, J. J. & Hulet, R. G. Evidence of Bose-Einstein Condensation in an Atomic Gas with Attractive Interactions. *Phys Rev Lett* **75,** 1687–1690 (1995).
11. Klaers, J., Schmitt, J., Vewinger, F. & Weitz, M. Bose-Einstein condensation of photons in an optical microcavity. *Nature* **468,** 545–548 (2010).
12. Landau, L. Theory of the Superfluidity of Helium II. *Phys Rev* **60,** 356–358 (1941).
13. Amo, A. *et al.* Superfluidity of polaritons in semiconductor microcavities. *Nat Phys* **5,** 805–810 (2009).
14. Sanvitto, D. *et al.* Persistent currents and quantized vortices in a polariton superfluid. *Nat Phys* **6,** 527–533 (2010).
15. Imamogıfmmode\bar\else¯\filu, A., Ram, R. J., Pau, S. & Yamamoto, Y. Nonequilibrium condensates and lasers without inversion: Exciton-polariton lasers. *Phys Rev A* **53,** 4250–4253 (1996).
16. Bhattacharya, P., Xiao, B., Das, A., Bhowmick, S. & Heo, J. Solid State Electrically Injected Exciton-Polariton Laser. *Phys Rev Lett* **110,** 206403 (2013).
17. Byrnes, T., Kim, N. Y. & Yamamoto, Y. Exciton-polariton condensates. *Nat Phys* **10,** 803–813 (2014).
18. Deng, H., Haug, H. & Yamamoto, Y. Exciton-polariton Bose-Einstein condensation. *Rev Mod Phys* **82,** 1489–1537 (2010).
19. Utsunomiya, S. *et al.* Observation of Bogoliubov excitations in exciton-polariton condensates. *Nat Phys* **4,** 700–705 (2008).

20. Berman, O. L., Kezerashvili, R. Y., Lozovik, Y. E. & Snoke, D. W. Bose–Einstein condensation and superfluidity of trapped polaritons in graphene and quantum wells embedded in a microcavity. *Philos. Trans. R. Soc. Lond. Math. Phys. Eng. Sci.* **368,** 5459–5482 (2010).
21. Lagoudakis, K. G. *et al.* Quantized vortices in an exciton-polariton condensate. *Nat Phys* **4,** 706–710 (2008).
22. Sanvitto, D. & Kena-Cohen, S. The road towards polaritonic devices. *Nat Mater* **15,** 1061–1073 (2016).
23. AmoA. *et al.* Exciton-polariton spin switches. *Nat Photon* **4,** 361–366 (2010).
24. Miller, D. A. B. Are optical transistors the logical next step? *Nat Photon* **4,** 3–5 (2010).
25. Plumhof, J. D., Stöferle, T., Mai, L., Scherf, U. & Mahrt, R. F. Room-temperature Bose–Einstein condensation of cavity exciton–polaritons in a polymer. *Nat Mater* **13,** 247–252 (2014).
26. Lerario, G. et al. Room-temperature superfluidity in a polariton condensate. *ArXiv160903153 Cond-Matquant-Gas* (2016).
27. Michetti, P., Mazza, L. & La Rocca, G. C. in *Organic Nanophotonics: Fundamentals and Applications* (ed. Zhao, Y. S.) 39–68 (Springer Berlin Heidelberg, 2015).
28. Splendiani, A. *et al.* Emerging Photoluminescence in Monolayer MoS2. *Nano Lett.* **10,** 1271–1275 (2010).
29. Mak, K. F., Lee, C., Hone, J., Shan, J. & Heinz, T. F. Atomically Thin MoS2: A New Direct-Gap Semiconductor. *Phys Rev Lett* **105,** 136805 (2010).
30. Zeng, H., Dai, J., Yao, W., Xiao, D. & Cui, X. Valley polarization in MoS2 monolayers by optical pumping. *Nat Nano* **7,** 490–493 (2012).
31. Wang, H. *et al.* Radiative lifetimes of excitons and trions in monolayers of the metal dichalcogenide MoS2. *Phys Rev B* **93,** 45407 (2016).
32. Palummo, M., Bernardi, M. & Grossman, J. C. Exciton Radiative Lifetimes in Two-Dimensional Transition Metal Dichalcogenides. *Nano Lett.* **15,** 2794–2800 (2015).
33. N Lundt and A Maryński and E Cherotchenko and A Pant and X Fan and S Tongay and G Sęk and A V Kavokin and S Höfling and C Schneider. Monolayered MoSe 2 : a candidate for room temperature polaritonics. *2D Mater.* **4,** 15006 (2017).
34. Dufferwiel, S. *et al.* Exciton-polaritons in van der Waals heterostructures embedded in tunable microcavities. *Nat Commun* **6,** (2015).
35. Wang, S. *et al.* Coherent Coupling of WS2 Monolayers with Metallic Photonic Nanostructures at Room Temperature. *Nano Lett.* **16,** 4368–4374 (2016).
36. Flatten, L. C. *et al.* Electrically tunable organic–inorganic hybrid polaritons with monolayer WS2. *Nat. Commun.* **8,** 14097 (2017).
37. Flatten, L. C. *et al.* Room-temperature exciton-polaritons with two-dimensional WS2. *Sci. Rep.* **6,** 33134 (2016).
38. Kleemann, M. et. al. Strong-coupling of WSe2 in ultra-compact plasmonic nanocavities at room temperature. *ArXiv170402756 Physicsoptics* (2017).
39. Wen, J. et. al. Room-temperature vacuum Rabi splitting with active control in two-dimensional atomic crystals. *ArXiv170307129 Physicsoptics* 21 Mar 2017
40. Walker, P. M. *et al.* Ultra-low-power hybrid light–matter solitons. *Nat. Commun.* **6,** 8317 (2015).
41. Das, A., Bhattacharya, P., Heo, J., Banerjee, A. & Guo, W. Polariton Bose–Einstein condensate at room temperature in an Al(Ga)N nanowire–dielectric microcavity with a spatial potential trap. *Proc. Natl. Acad. Sci.* **110,** 2735–2740 (2013).

42. Walker, P. M. *et al.* Exciton polaritons in semiconductor waveguides. *Appl. Phys. Lett.* **102,** 12109 (2013).
43. Jorda, S. Exciton polaritons in quantum wells embedded in waveguides and microcavities. *J. Opt. Soc. Am. B* **13,** 1054–1060 (1996).
44. in 385 ((Wiley India Pvt. Limited, 2007).).
45. Savona, V., Andreani, L. C., Schwendimann, P. & Quattropani, A. Quantum well excitons in semiconductor microcavities: Unified treatment of weak and strong coupling regimes. *Solid State Commun.* **93,** 733–739 (1995).
46. Selig, M. *et al.* Excitonic linewidth and coherence lifetime in monolayer transition metal dichalcogenides. *Nat. Commun.* **7,** 13279 (2016).
47. Feldmann, J. *et al.* Linewidth dependence of radiative exciton lifetimes in quantum wells. *Phys Rev Lett* **59,** 2337–2340 (1987).
48. Sanders, G. D. & Chang, Y.-C. Radiative decay of the bound exciton in direct-gap semiconductors: The correlation effect. *Phys Rev B* **28,** 5887–5896 (1983).
49. Flatten, L. C. *et al.* Room-temperature exciton-polaritons with two-dimensional WS2. *Sci. Rep.* **6,** 33134 (2016).
50. Sorger, V. J. *et al.* Strongly Enhanced Molecular Fluorescence inside a Nanoscale Waveguide Gap. *Nano Lett.* **11,** 4907–4911 (2011).
51. Saba, M. *et al.* High-temperature ultrafast polariton parametric amplification in semiconductor microcavities. *Nature* **414,** 731–735 (2001).
52. Guimarães, M. H. D. *et al.* Atomically Thin Ohmic Edge Contacts Between Two-Dimensional Materials. *ACS Nano* **10,** 6392–6399 (2016).
53. Yuan, H. *et al.* Polarization-sensitive broadband photodetector using a black phosphorus vertical p–n junction. *Nat Nano* **10,** 707–713 (2015).
54. Chen Xia, Li Chao & Tsang Hon K. Device engineering for silicon photonics. *NPG Asia Mater* **3,** 34–40 (2011).
55. Michel, J., Liu, J. & Kimerling, L. C. High-performance Ge-on-Si photodetectors. *Nat Photon* **4,** 527–534 (2010).
56. Zuocheng Zhang, Likai Li, Jason Horng, Nai Zhou Wang, Fangyuan Yang, Yijun Yu, Yu Zhang, Guorui Chen, Kenji Watanabe, Takashi Taniguchi, Xian Hui Chen,Feng Wang, Yuanbo Zhang. Strain-Modulated Bandgap and Piezo-Resistive Effect in Black Phosphorus Field-Effect Transistors. Nano Lett. 17, 10, 6097-6103
57. Geim, A. K. & Grigorieva, I. V. Van der Waals heterostructures. *Nature* **499,** 419–425 (2013).